Available online at www.sciencedirect.com
SCIENCE DIRECT®
Journal of Applied Geophysics 52 (2003) 177–191
JOURNAL OF APPLIED GEOPHYSICS
www.elsevier.com/locate/jappgeo

Acoustic and electromagnetic properties of soils saturated with salt water and NAPL

José M. Carcione*, Géza Seriani, Davide Gei

Istituto Nazionale di Oceanografia e di Geofisica Sperimentale-OGS, Borgo Grotta Gigante 42c, 34010 Sgonico, Trieste, Italy

Received 25 June 2002; accepted 14 January 2003

Abstract

Electrical, seismic, and electromagnetic methods can be used for noninvasive determination of subsurface physical and chemical properties. In particular, we consider the evaluation of water salinity and the detection of surface contaminants. Most of the relevant properties are represented by electric conductivity, P-wave velocity, and dielectric permittivity. Hence, it is important to obtain relationships between these measurable physical quantities and soil composition, saturation, and frequency. Conductivity in the geoelectric frequency range is obtained with Pride's model for a porous rock. (The model considers salinity and permeability.) White's model of patchy saturation is used to calculate the P-wave velocity and attenuation. Four cases are considered: light nonaqueous phase liquid (LNAPL) pockets in water, dense nonaqueous phase liquid (DNAPL) pockets in water, LNAPL pockets in air, and DNAPL pockets in air. The size of the pockets (or pools), with respect to the signal wavelength, is modeled by the theory. The electromagnetic properties in the GPR frequency range are obtained by using the Hanai–Bruggeman equation for two solids (sand and clay grains) and two fluids (LNAPL or DNAPL in water or air). The Hanai–Bruggeman exponent (1/3 for spherical particles) is used as a fitting parameter and evaluated for a sand/clay mixture saturated with water.

Pride's model predicts increasing conductivity for increasing salinity and decreasing permeability. The best-fit exponent of the Hanai–Bruggeman equation for a sand/clay mixture saturated with water is 0.61, indicating that the shape of the grains has a significant influence on the electromagnetic properties. At radar frequencies, it is possible to distinguish between a water-saturated medium and a NAPL-saturated medium, but LNAPL- and DNAPL-saturated media have very similar electromagnetic properties. The type of contaminant can be better distinguished from the acoustic properties. P-wave velocity increases with frequency, and has dissimilar behaviour for wet and dry soils.

Keywords: Acoustic; Electromagnetic; Soil; LNAPL; DNAPL; GPR; Seismic

1. Introduction

Contaminants in the soil may exist in the gas phase, in the aqueous phase, and/or as a separate, immiscible liquid phase [i.e, nonaqueous phase liquids (NAPLs)]. Dense NAPL (DNAPL) consists of a solution of organic compounds (e.g., chlorinated hydrocarbons) denser than water. DNAPLs sink to the bottom of the aquifer. On the other hand, light NAPL (LNAPL) consists of a solution of organic compounds (e.g., petroleum hydrocarbons) which is less dense than

* Corresponding author. Fax: +39-40-327521.
E-mail address: jcarcione@ogs.trieste.it (J.M. Carcione).

0926-9851/03/$ - see front matter © 2003 Elsevier Science B.V. All rights reserved.
doi:10.1016/S0926-9851(03)00012-0

water and forms a layer that floats on the surface of the groundwater table. Because NAPLs are immiscible fluids, they may exist as pools, implying patchy, nonuniform saturation. The flow of seawater into fresh water aquifers and the injection of brine into the subsurface through hydrocarbon production wells constitute another major problem affecting the quality of industrial and domestic water supplies.

Geophysical methods allow noninvasive determination of subsurface physical and chemical properties. Seismic, electrical, magnetic, and GPR have been applied with success to site characterization. The use of integrated geophysical methods has found innovative uses at hazardous waste sites (e.g., Clement et al., 1997; Hubbard et al., 1997). They are able to detect the presence of either dense or light, nonaqueous phase liquids (D/LNPALs) (Greenhouse et al., 1993; Daniels et al., 1995; Valle and Carcione, submitted for publication), and, with the use of rock physics, can map water content and salinity (Senechal et al., 2000; Hagrey and Müller, 2000). Hence, it is fundamental to establish relationships between soil composition, saturation, and geophysical parameters since this investigation will provide new methods to interpret geophysical field data.

Seismic measurements provide P- and S-wave velocity and attenuation (quality factor), while electromagnetic data provide electromagnetic velocity and attenuation, which can be translated to dielectric constant and conductivity. The study of the effects of saturation and fluid type requires to model the soil as a porous medium. There are two main theories which predict the dependence of wave velocity and attenuation as a function of frequency and patchy saturation: White's model (White, 1975; Mavko et al., 1998, p. 207) and the theory illustrated by Akbar et al. (1994) and Dvorkin et al. (1995). The fluid effects on wave velocity and attenuation depend on the frequency range. At low frequencies, the fluid has enough time to achieve pressure equilibration (relaxed regime), and Gassmann's modulus properly describes the saturated bulk modulus. At high frequencies, the fluid cannot relax and this state of unrelaxation induces pore pressure gradients. Consequently, the bulk and shear moduli are stiffer than at low frequencies. Dvorkin et al.'s (1995) model is based on the assumption that the rock is fully saturated, while Akbar et al. (1994) includes the effects of partial saturation.

To model the acoustic properties of soils, we use White's model (White, 1975; Mavko et al., 1998). This model describes wave velocity and attenuation as a function of frequency, pool size, and soil permeability. Attenuation and velocity dispersion are caused by fluid flow between patches of different pore pressures. The critical fluid diffusion relaxation scale is proportional to the square root of the ratio permeability to frequency. At seismic frequencies, the length scale is very large, and the pressure is nearly uniform throughout the medium, but as frequency increases, pore pressure differences can cause an important increase in P-wave velocity. The advantage of White's model is that there is no need to include new parameters, such as length scales or relaxation times that describe squirt-flow effects. The theory, based on Biot's theory of poroelasticity, predicts that increasing fluid viscosity or decreasing permeability shifts the relaxation peaks towards lower frequencies. Then, a correct use of Biot's theory (i.e., including the effects of fluid distribution heterogeneity) allows to predict the behavior of observed experimental data. White's model is generalized here to include the effects of clay and the presence of dissipation mechanism of different nature.

Few theoretical models have been proposed to describe contaminant fluid behavior and its effects on GPR response. Endres and Redman (1993) developed a pore-scale fluid model for clay-free granular soils, and Sen et al. (1981) used a self-similar theory, which guarantees the continuity of the water-filled pore space, in agreement with Archie's (1942) law. The electromagnetic properties of soils are modeled with the self-similar theory. Carcione and Seriani (2000) used this theory for computing the effective dielectric permittivity and conductivity of sand/clay mixtures saturated with air, water, and hydrocarbon. They consider anisotropic clay layers and spherical inclusions. Here, we assume an isotropic constitutive equation and arbitrary pore and grain geometries (the exponent of the Hanai–Bruggeman equation is used as a fitting parameter). Salinity can be obtained from electric conductivity by using Pride's model (Pride, 1994; Senechal et al., 2000). Pride derived an equation for the conductivity by using the volume averaging method.

Rock-physics models can be combined with numerical modeling methods (Carcione, 1996a,b,

2001) to investigate the sensitivity of the wave field on the soil properties and conditions (porosity, saturation, fluid content and distribution, etc.).

The objective of this work is to obtain relationships between measurable physical quantities and soil composition, saturation, and frequency, in particular for the evaluation of water salinity and the detection of surface contaminants. The paper is organized as follows. In Section 2, we introduce the general expressions of the phase velocity and quality factor as a function of the complex velocity (acoustic and electromagnetic, where acoustic refers to seismic, sonic, or ultrasonic). In Section 3, we consider the electrical conductivity in the geoelectric frequency range, and analyze the effects of water salinity and soil permeability. Section 4 discusses the effects of NAPL saturation on the electromagnetic properties in the radar (GPR) frequency range. Finally, in Section 5, we study the effects of NAPL saturation on the acoustic properties, from the seismic to the ultrasonic range.

2. Velocity and attenuation

The concept of complex velocity can be used to obtain the phase velocity and attenuation of the acoustic and electromagnetic fields. Let V be either the acoustic complex velocity (V_P and V_S for P- and S-waves, respectively) or the electromagnetic complex velocity [$V = 1/\sqrt{\mu_0 \epsilon}$, where μ_0 is the magnetic permeability of vacuum (see Table 1) and ϵ is the complex dielectric permittivity]. Then, the phase velocity and quality factor are given by

$$c = \left[\mathrm{Re}\left(\frac{1}{V}\right)\right]^{-1} \tag{1}$$

and

$$Q = \frac{\mathrm{Re}(V^2)}{\mathrm{Im}(V^2)} \tag{2}$$

(e.g., Carcione, 2001), where Re and Im denote real and imaginary parts, respectively.

Table 1
Physical properties (optical permittivity, electrical conductivity, P-wave and S-wave velocities, density, and viscosity)

Medium	ϵ^∞ (ϵ_0)	σ (S/m)	c_P (m/s)	c_S (m/s)	ρ (kg/m^3)	η (Pa s)
Quartz	5	0	6050	4090	2650	–
Clay (wet)	30	0.1	2000	1400	1400	–
Air (gas)	1	0	330	0	1.18	0.00002
Fresh water	4.23	0.0016[a]	1440	0	1000	0.001
Salt water	4.23	0.41[b]	1500	0	1036	0.003
LNAPL (gasoline)	2	10^{-6}	1200	0	750	0.0004
DNAPL (perchloro-ethylene)	2.3	10^{-7}	1600	0	1620	0.0008

Sources: Angenheister (1982), Carmichael (1989), Clark (1966), Mavko et al. (1998), Schön (1996), and Wensink (1993).
$\epsilon_0 = 8.85 \times 10^{-12}$ F/m; $\mu_0 = 4\pi \times 10^{-7}$ H/m.
[a] 0.01 ppt of NaCl.
[b] 2.6 ppt of NaCl.

3. Conductivity versus salinity

The electrical conductivity of a porous soil as a function of salinity and hydraulic permeability is obtained by using Pride's (1994) model. The expression of the electric conductivity is

$$\bar{\sigma} = \left(\frac{\phi \sigma_f}{\mathcal{T}}\right)\left[1 + \frac{2[C_{em} + \mathrm{Re}(C_{os}(\omega))]}{\sigma_f \Lambda}\right] \tag{3}$$

(see Eq. (A-1)), where ω is the angular frequency, ϕ is the porosity, σ_f is the fluid (ionic) conductivity (Eq. (A-2)), $\mathcal{T}$ is the tortuosity, and Λ is a geometrical parameter related to the surface-to-pore volume ratio (see Eq. (B-19)). Moreover, C_{em} is the excess conductance associated with the electromigration of double-layer ions and C_{os} is the electro-osmotic conductance (see Appendix A.1).

Let us consider a frequency of 100 kHz, temperature $T = 15$ °C, water viscosity $\eta_f = 1$ cP, water density $\rho_f = 1000$ kg/m^3 (fresh water), tortuosity $\mathcal{T} = 2.5$, $\xi = 8$, and porosity $\phi = 0.3$ ($\mathcal{T}$ and ξ are parameters related to the geometry of the pore space; e.g., Carcione, 2001, p. 242; Johnson et al., 1987). Fig. 1a shows the conductivity as a function of salinity for sand (κ, permeability = 500 mD, dotted line) and clay ($\kappa = 5 \times 10^{-6}$ mD, dashed line). The symbols represent experimental data obtained by Rhoades (1980) for Dateland soil (fine sandy loam) (see Rhoades et al., 1999). Rhoades provides the conduc-

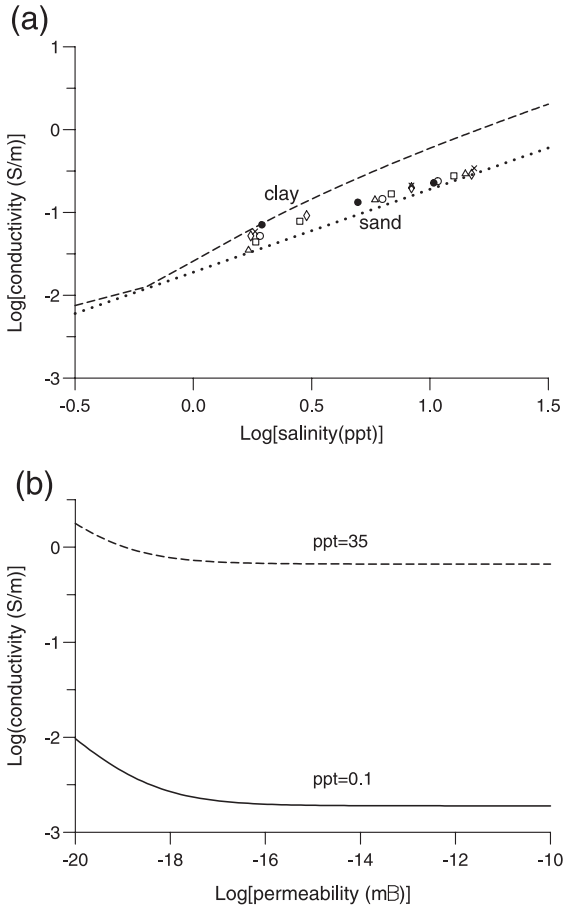

Fig. 1. (a) Conductivity as a function of salinity for sand (κ, permeability = 500 mD, dotted line) and clay ($\kappa = 5 \times 10^{-6}$ mD, dashed line). The symbols correspond to measurements obtained by Rhoades (1980). (b) The figure shows conductivity versus permeability, where the solid line corresponds to fresh water and the dashed line to salt water.

tivity of the saturation extract (saturating fluid) versus the conductivity of the soil. We have used Eq. (A-2) to relate the conductivity of the saturating fluid to the salinity. The conductivity versus permeability is shown in Fig. 1b, where the solid line corresponds to fresh water and the dashed line to salt water. The contribution of the excess conductance associated with the electromigration of double-layer ions and the electro-osmotic conductance is significant in clays (second term of the right-hand-side of Eq. (A-1)). Permeability κ plays a key role because the surface-to-volume ratio $2/\Lambda$ is large (see Eq. (B-19)), and Λ is smaller than in sands. As expected, conductivity increases with increasing salinity and decreasing permeability.

Table 2
Properties of the sand/clay mixture

Sample	Sand %	Clay %	Water %	Permittivity (ϵ_0)	Conductivity (S/m)
1	66	0	34	12.1	0.006
2	61	0	39	14.1	0.011
3	63	4	33	16.4	0.083
4	57	1	42	18.1	0.040
5	59	4	37	20.2	0.094
6	38	7	55	32.3	0.20
7	15	7	78	49.7	0.28
8	8	8	84	52.8	0.29
9	0	10	90	62.6	0.40

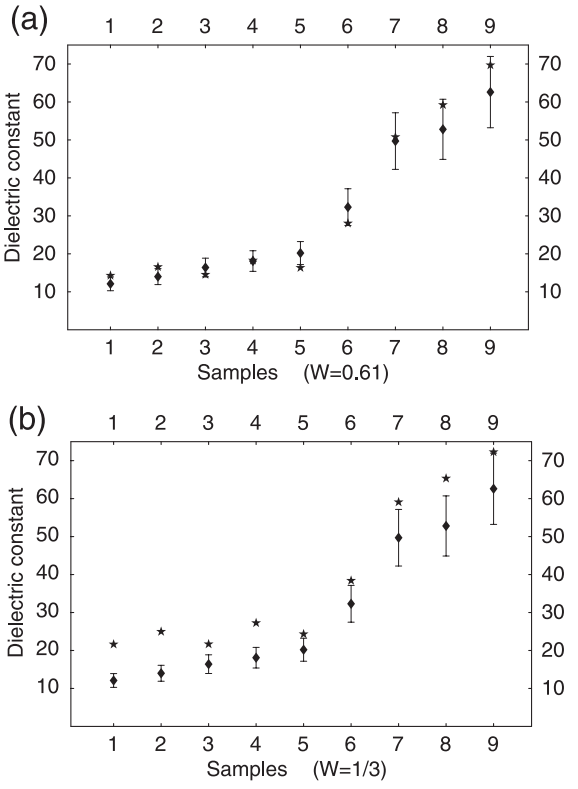

Fig. 2. Comparison between the computed (star) and measured (diamond) effective permittivity for $W = 0.61$ (a) and $W = 1/3$ (b). Measured data are from Table 2, and a relative error of 15% is shown by using error bars.

4. Electromagnetic velocity and conductivity

To obtain the Hanai–Bruggeman exponent W of Eq. (A-13), we fit the dielectric permittivity and conductivity of a sand/clay mixture saturated with water (Schön, 1996, p. 469). Sand is pure silica sand, clay is Na-montmorillonite, and water is distilled deionized water. Their properties are given in Table 1. Table 2 shows the data for a frequency of 100 MHz. The data have been transformed from weight percentage to volume percentage by assuming a density of 2650 kg/m^3 for the sand grains and 2608 kg/m^3 (Carmichael, 1989) for the clay grains. The conductivity has been obtained from the loss tangent. If ϵ is the complex dielectric constant, the loss tangent is defined as $\omega\sigma_e/\epsilon_e$, where ω is the angular frequency and ϵ_e and σ_e are the effective permittivity and conductivity, respectively, given in the table. Figs. 2 and 3 show the dielectric constant and conductivity for $W=0.61$ (a) and $W=1/3$ (b), where 0.61 is the best fit to the experimental data. The Hanai–Bruggeman exponent is $W=1/3$ for spherical particles. The fact that $W\neq 1/3$ but equal to 0.61 indicates a significant departure of the grain shape from a sphere. Then, the exponent $W=0.61$ is used in the next calculations to obtain the electromagnetic properties of a sand saturated with aviation gasoline (LNAPL), air, and water.

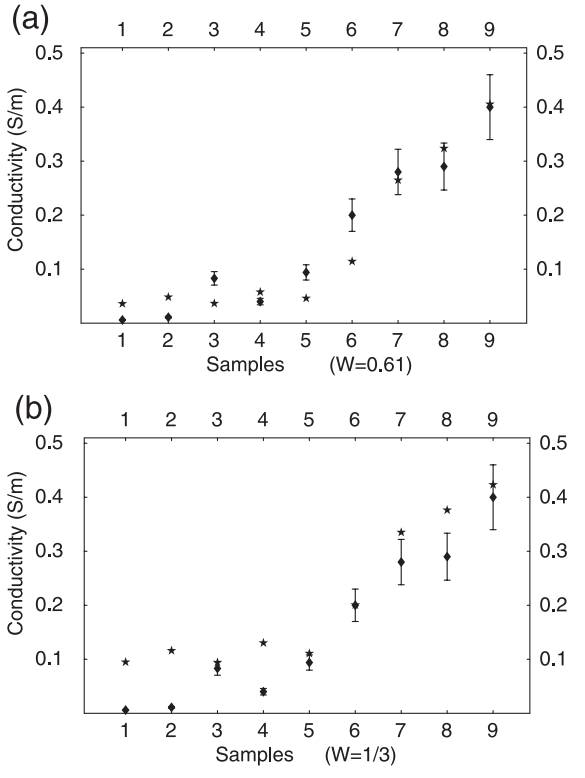

Fig. 3. Comparison between the computed (star) and measured (diamond) effective conductivity for $W=0.61$ (a) and $W=1/3$ (b). Measured data are from Table 2, and a relative error of 15% is shown by using error bars.

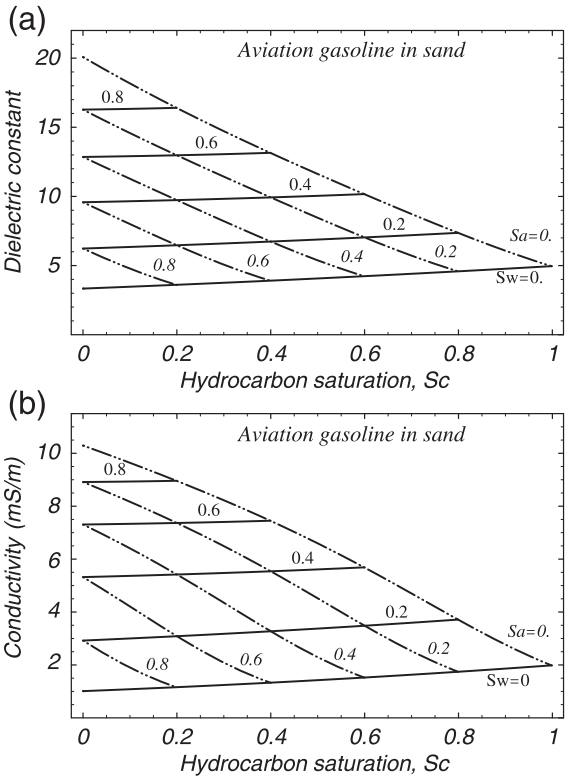

Fig. 4. Effective permittivity (a) and effective conductivity (b) for sand partially saturated with LNAPL, water, and air versus LNAPL saturation. The thick continuous lines correspond to constant fresh (rain) water saturation S_w (Roman numbers), while the thick broken lines correspond to constant air saturation S_a (italic numbers).

Fig. 4 represents $\epsilon_e=\mathrm{Re}(\epsilon)$ (a) and $\sigma_e=\omega\mathrm{Im}(\epsilon)$ (b) for sand partially saturated with LNAPL, fresh water, and air. The thick continuous lines correspond to constant water saturation (Roman numbers), while the thick broken lines correspond to constant air saturation (italic numbers). For instance, if contaminant saturation $S_c=0.4$ and water saturation $S_w=0.4$, the saturation of air is $S_a=1-S_w-S_c=0.2$, giving an

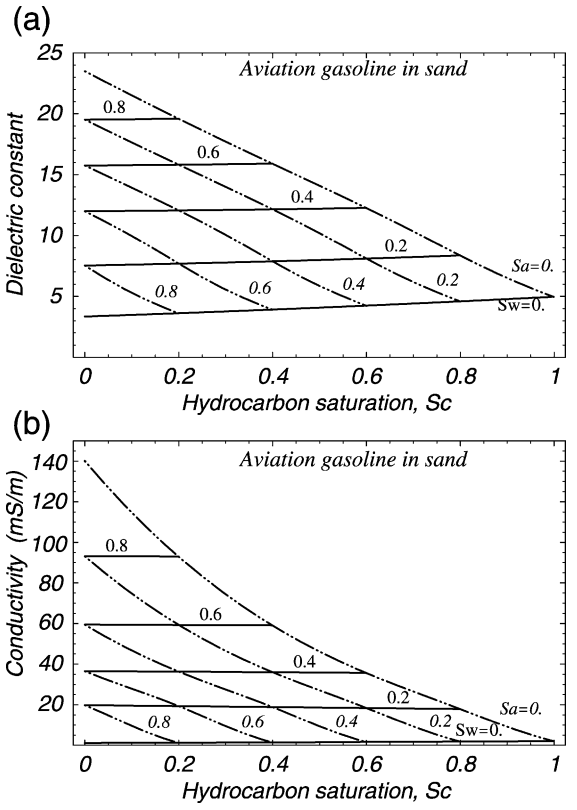

Fig. 5. Effective permittivity (a) and effective conductivity (b) for sand partially saturated with LNAPL, water, and air versus LNAPL saturation. The thick continuous lines correspond to constant salt water saturation S_w (Roman numbers), while the thick broken lines correspond to constant air saturation S_a (italic numbers).

effective dielectric constant equal to $10\epsilon_0$. Soil fully saturated with water ($S_w = 1$) has a permittivity of $20\epsilon_0$; full air saturation corresponds to $S_w = S_c = 0$, with a permittivity of $3\epsilon_0$ (the lower value of the curve $S_w = 0$); full LNAPL saturation, i.e., $S_c = 1$, implies a permittivity of nearly $5\epsilon_0$ (the higher value of the curve $S_w = 0$). For a given water saturation, the dielectric constant increases with increasing NAPL saturation since NAPL has a higher permittivity than air. The same argument holds for the effective conductivity. This effect is more pronounced for increasing water content since water has a much higher permittivity than NAPL ($78\epsilon_0$ versus $2\epsilon_0$). The same curves for salt water are shown in Fig. 5. The medium has higher permittivity and conductivity. Substitution of LNAPL with DNAPL has not a major effect on these curves since the electromagnetic properties are comparable.

5. P-wave velocity and attenuation

White's model yields the P-wave velocity for a partially saturated soil (Appendix B, Eq. (B-2)). Let

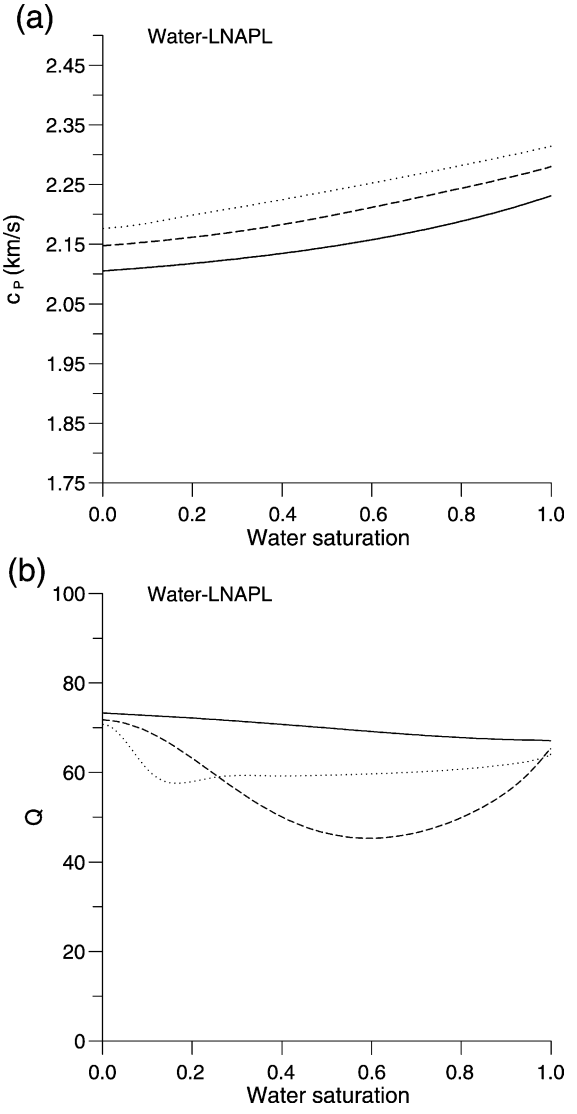

Fig. 6. P-wave velocity (a) and quality factor (b) versus water saturation for LNAPL pockets in water-saturated soil. The solid, dashed, and dotted lines correspond to 50 Hz, 5, and 100 kHz, respectively.

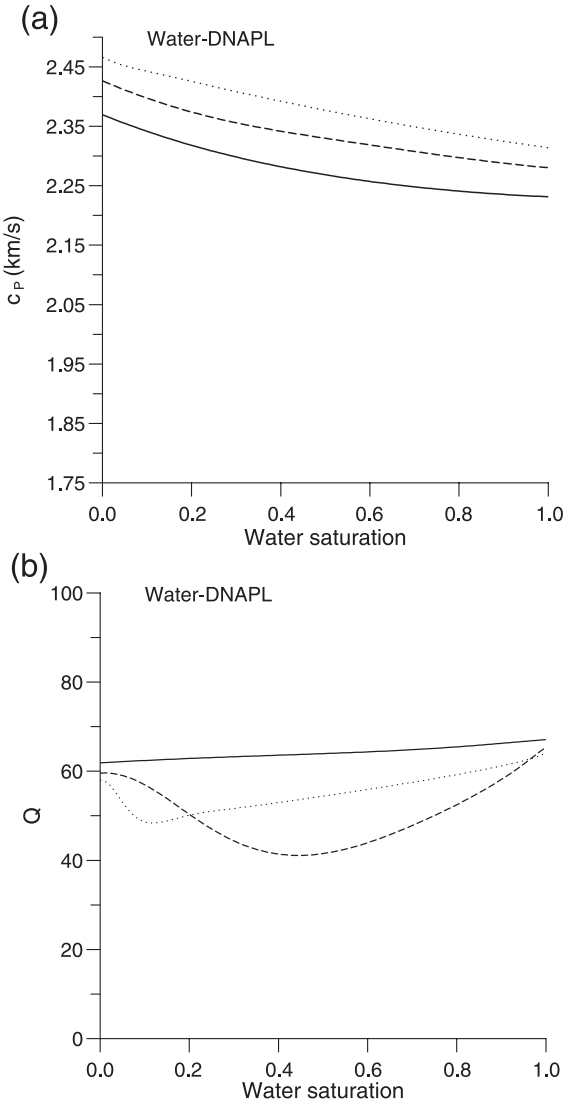

Fig. 7. P-wave velocity (a) and quality factor (b) versus water saturation for DNAPL pockets in water-saturated soil. The solid, dashed, and dotted lines correspond to 50 Hz, 5, and 100 kHz, respectively.

us consider a soil with a clay content $C=0.3$, porosity $\phi=0.35$, tortuosity $\mathscr{T}=2.5$, permeability $\kappa=550$ mD, and $\xi=8$. According to Table 1 and the theory illustrated in Appendix B, we obtain $K_q=38$ GPa, $\mu_q=44$ GPa (sand grains), $K_c=3.7$ GPa, $\mu_c=5.2$ GPa (clay particles), $K_s=17.6$ GPa, $\mu_s=22.3$ GPa (composite grain moduli), and dry-soil moduli $K_m=3.05$ GPa, and $\mu_m=22.3$ GPa. Assume that the size of the pockets is $b=4$ cm (see Eq. (B-1)), and that we parameterize the viscoelastic attenuation with $Q_\kappa=100$ and $f_0=100$ kHz (see Appendix B.2).

Figs. 6 and 7 show the P-wave velocity (a) and quality factor (b) versus fluid saturation for LNAPL pockets and DNAPL pockets in water, respectively. The solid, dashed, and dotted lines correspond to 50 Hz, 5, and 100 kHz, respectively.

To our knowledge, there are no published experimental data about velocity and attenuation of media partially saturated with NAPL. Similar relevant data have been published in the field of exploration geophysics, regarding rocks saturated with water and reservoir gas. For instance, Fig. 8 shows measurements, at different saturations and frequencies, performed by Cadoret et al. (1995) (limestones) and King et al. (2000) (sandstones). The plots show higher velocities at high frequencies, in agreement with the predictions of White's model. Although these measurements are performed at different pressure conditions and for different fluid types compared to those of the present study, our model should be able to predict the qualitative behaviour of the curves. These data can be compared to the curves shown in Figs. 9a and 10a, corresponding to LNAPL pockets and DNAPL pockets in air, respectively. The solid, dashed, and dotted

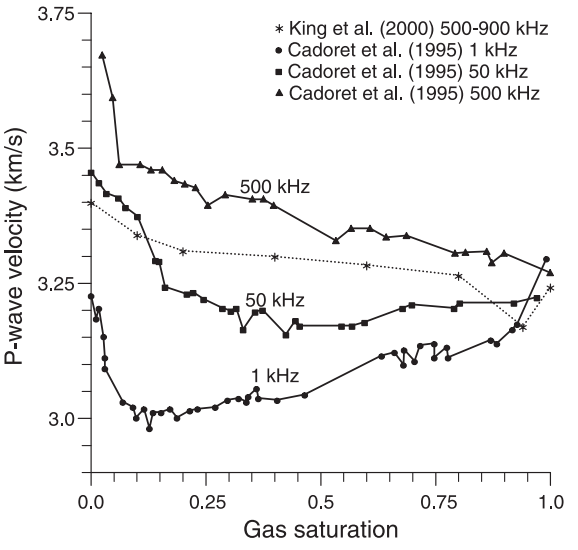

Fig. 8. Measurements of P-wave velocities versus gas saturation at different frequencies, performed by Cadoret et al. (1995) (limestones) and King et al. (2000) (sandstones).

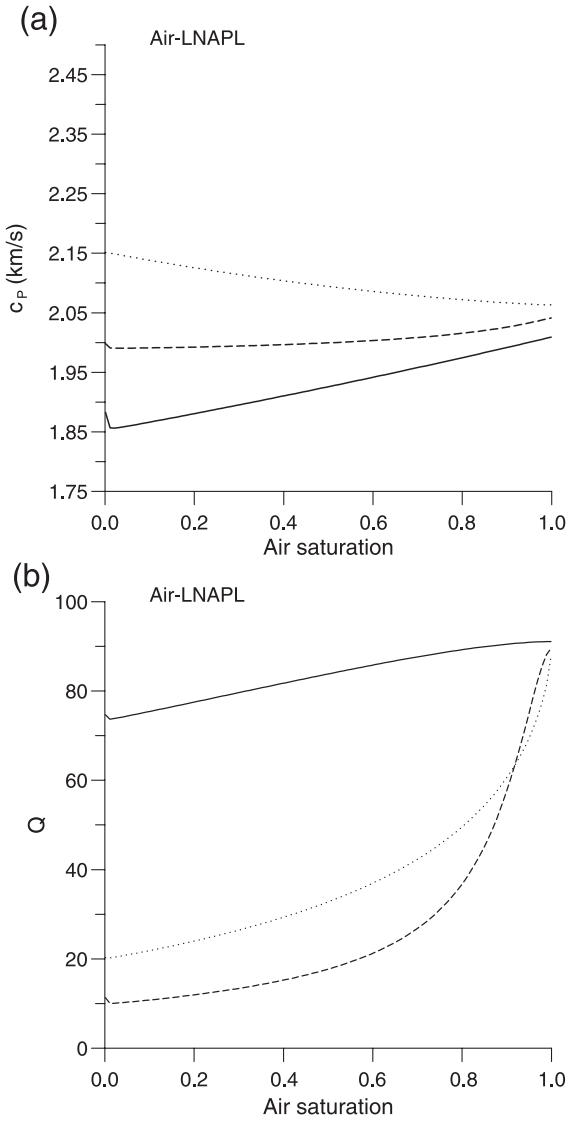

Fig. 9. P-wave velocity (a) and quality factor (b) versus air saturation for LNAPL pockets in air-saturated soil. The solid, dashed, and dotted lines correspond to 50 Hz, 5, and 100 kHz, respectively.

lines correspond to 50 Hz, 5, and 100 kHz, respectively.

An analysis of (Figs. 6, 7, 9, and 10) follows. The phase velocity increases with decreasing LNAPL and increasing DNAPL content, when the soil is saturated with water (see Figs. 6a and 7a). When the saturating medium is air, the behaviour depends on frequency. At seismic frequencies, the phase velocity decreases with increasing NAPL saturation (see Fig. 9a and b). Increasing the frequency implies higher velocity in all cases, in agreement with Fig. 8. In general, the Q factors decrease with increasing frequency (attenuation increases). In dry soils (Figs. 9b and 10b), the attenuation is larger for full NAPL saturation. In wet

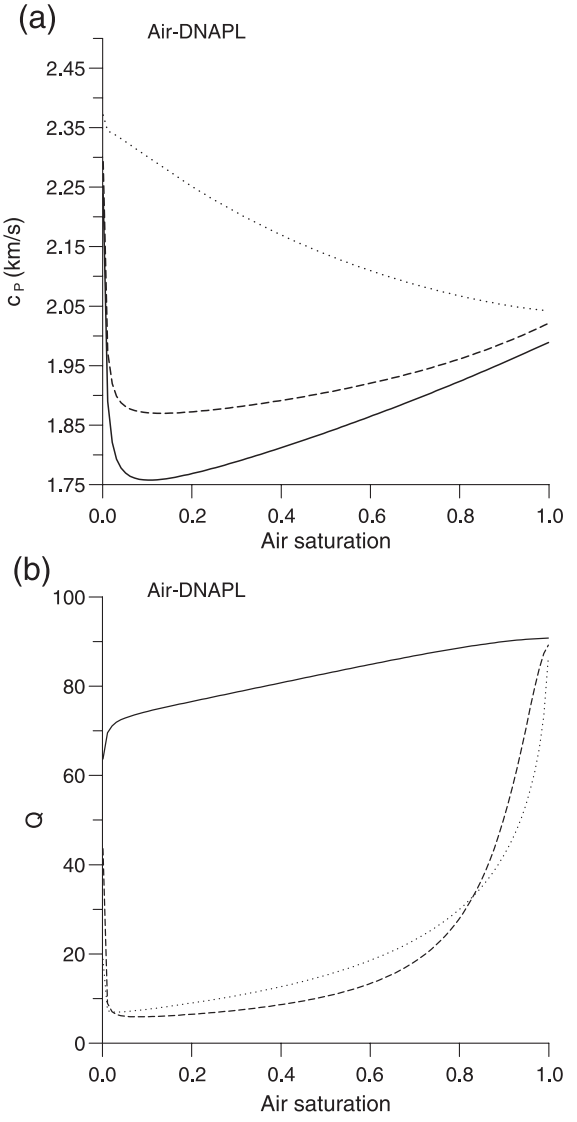

Fig. 10. P-wave velocity (a) and quality factor (b) versus air saturation for DNAPL pockets in air-saturated soil. The solid, dashed, and dotted lines correspond to 50 Hz, 5, and 100 kHz, respectively.

soils and seismic frequencies (Figs. 6b and 7b), attenuation is almost constant with saturation.

Let us consider the case illustrated in Fig. 7, assuming a constant DNAPL saturation of 30%. Fig. 11 shows the P-wave velocity and attenuation for 300 Hz as a function of the patch size b. As can be seen, there is a relaxation mechanism at approximately 1 cm.

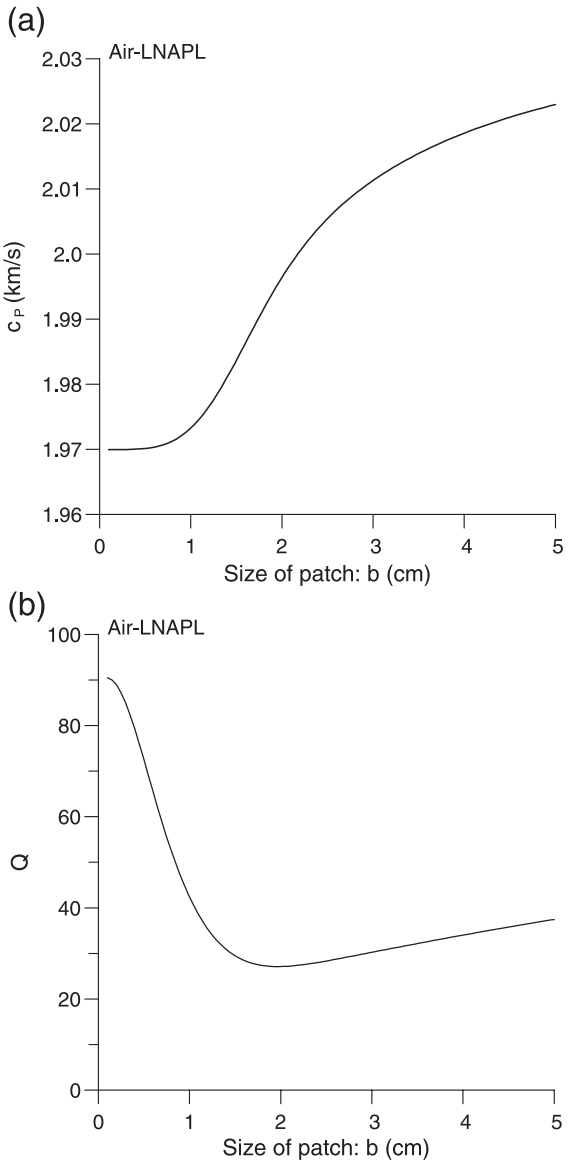

Fig. 11. P-wave velocity and attenuation (quality factor) for 300 Hz as a function of the patch size b. A constant LNAPL saturation of 30% is considered.

The transition frequency separating the relaxed and unrelaxed states, which is the location of the relaxation peak, is approximately given by

$$f_c = \frac{\kappa K_{E2}}{\pi \eta_2 b^2}, \tag{4}$$

where κ is the permeability, K_{E2} is given in Eq. (B-6), and η_2 is the viscosity of air (e.g., Mavko et al., 1998, p. 209). Hence, the approximate critical size of the patch should be

$$b_c = \sqrt{\frac{\kappa K_{E2}}{\pi \eta_2 f_c}}, \tag{5}$$

which gives a value of 0.33 cm.

6. Conclusions

The acoustic and electromagnetic properties of soils saturated with air, water, and hydrocarbons show significant variations, depending on the degree of saturation of the different fluids.

Conductivity increases with increasing salinity and decreasing permeability (clayey soils are more conductive than sandy soils). At radar frequencies, the departure of the grain shape of a sand/clay mixture from a sphere is evidenced by the value of the best-fit Hanai–Bruggeman exponent (0.61 versus 1/3 for spheres). For a given water saturation, the dielectric constant increases with increasing NAPL saturation since NAPL has a higher permittivity than air. The same argument holds for the effective conductivity. This effect is more pronounced for increasing water content since water has a much higher permittivity than NAPL. Substitution of LNAPL with DNAPL has not a major effect on these curves since the electromagnetic properties are comparable.

P-wave phase velocity increases with decreasing LNAPL and increasing DNAPL content, when the soil is saturated with water. When the saturating medium is air, the behaviour depends on frequency. At seismic frequencies, the phase velocity decreases with increasing NAPL saturation. Increasing the frequency implies higher velocity in all cases. In general, the Q factors decrease with increasing frequency (attenuation increases). In dry soils, the attenuation is larger for full NAPL saturation. In wet soils and

seismic frequencies, attenuation is almost constant with saturation. There is a relaxation mechanism associated with the size of the contaminant pools. The dimension of the pools, associated to this mechanism, is of the order of tens of millimeters for LNAPL saturation in dry soils.

These features allow the use of seismic and electromagnetic techniques, such as GPR, for detecting and mapping pools of near-surface low-loss contaminants and evaluating the presence of saline waters in aquifers. The models can be used together with a full-wave modeling methods for computing radargrams. The models, properly calibrated with experimental data, and the simulation algorithm constitute a modeling tool for aiding in the interpretation of aquifers and hydrocarbon-contaminated soils.

Acknowledgements

This work was financed in part by the European Union under the HYGEIA project. We thank Steve Pride for helpful suggestions about his conductivity model. We are also grateful to Said Attia al Hagrey and an anonymous reviewer for useful comments.

Appendix A. Electromagnetic models

A.1. Pride's model for conductivity

Pride (1994) obtained an expression of the conductivity of a porous medium saturated with a fluid, containing a number of ionic species. (Salt water is a binary symmetric electrolyte, containing the cations Na^+ and the anions Cl^-.) Pride used volume-averaging methods to obtain the following expression:

$$\bar{\sigma} = \left(\frac{\phi\sigma_f}{\mathscr{T}}\right)\left[1 + \frac{2[C_{em} + \mathrm{Re}(C_{os}(\omega))]}{\sigma_f \Lambda}\right], \qquad (A-1)$$

where Re takes real part, ω is the angular frequency, ϕ is the porosity, σ_f is the fluid (ionic) conductivity, $\mathscr{T}$ is the tortuosity, and Λ can be obtained from Eq. (B-19). The fluid conductivity for two ions is given by

$$\sigma_f = \sum_{l=1}^{2} (ez_l)^2 b_l \mathscr{N}_l, \qquad (A-2)$$

where e is the electric charge of the ions, z_l is the valence (ez_l represents the net charge and sign of the ion), b_l is the mobility (units of velocity per unit force), and $\mathscr{N}_l$ is the bulk ionic concentration. Moreover,

$$C_{em} = 2d \sum_{l=1}^{2} (ez_l)^2 b_l \mathscr{N}_l \left[\exp\left(-\frac{ez_l\zeta}{2kT}\right) - 1\right] \qquad (A-3)$$

is the excess conductance associated with the electromigration of double-layer ions, and

$$C_{os} = \frac{(\epsilon_f\zeta)^2 P}{2d\eta_f}\left(1 - \frac{2i^{3/2}d}{P\delta}\right)^{-1} \qquad (A-4)$$

represents the conductance due to electrically induced streaming (convection) of the excess double-layer ions (the electro-osmotic conductance), where $i = \sqrt{-1}$, η_f is the fluid viscosity, d is the Debye length, which is a measure of the thickness of the diffuse double layer,

$$d = \left(\sum_{l=1}^{2} \frac{(ez_l)^2 \mathscr{N}_l}{\epsilon_f kT}\right)^{-1/2}, \qquad (A-5)$$

k is Boltzmann's constant (1.38×10^{-23} J/K), T is temperature in Kelvin, ϵ_f is the dielectric constant of the electrolyte, δ is the viscous skin depth,

$$\delta = \sqrt{\frac{\eta_f}{\omega\rho_f}}, \qquad (A-6)$$

where ρ_f is the fluid density (see Eq. (B-4)), ζ is the zeta potential, and

$$P = \frac{8kTd^2}{\epsilon_f\zeta^2} \sum_{l=1}^{2} \mathscr{N}_l \left[\exp\left(-\frac{ez_l\zeta}{2kT}\right) - 1\right]. \qquad (A-7)$$

The conductivity of pure water, without other ions than H^+ and OH^-, is 3.6×10^{-6} S/m (Schön, 1996, p. 394). Charge transport in salt water is due to impuric conduction of Na^+ and Cl^-. For salt water, $e = 1.6 \times 10^{-19}$ C, $z_1 = 1$ (cation), $z_2 = -1$ (anion), $\mathscr{N}_1 = \mathscr{N}_2 = \mathscr{N}$, and we consider $b_1 = b_2 = 3 \times 10^{11}$ N

s/m (a typical inorganic ion). The bulk ionic concentration is given by

$$\mathcal{N} = sN_a, \qquad (A-8)$$

where s is water salinity in mol/l and N_a is Avogadro's number (6.022×10^{23}/mol). The ζ potential is taken from experimental data on quartz. Pride and Morgan (1991) obtained the following expression as a function of salinity:

$$\zeta(V) = 0.008 + 0.026\log_{10}s. \qquad (A-9)$$

Salt concentration can be expressed in ppt (parts per thousand (o/oo)) and mol/l, where ppt = mass of NaCl (in g) in 1000 g of water. The relation is

$$\text{ppt} = \frac{58.443s}{\rho_w}, \qquad (A-10)$$

where 58.443 is the molecular mass of NaCl in g, s is the solution concentration in mol/l, and ρ_w is given in g/cm^3. The average value in seawater is 35 ppt. For fresh waters, the concentration is less than 1 ppt, and for brines, the concentration is greater than 35 ppt. Note that 1 mol/l = 58.443 kg/m^3 and that the Avogadro number per kilogram of NaCl is 1.03×10^{25}.

The contributions of C_{em} and C_{os} are not significant for clean sands, for which the volume-to-surface ratio is too large. Those terms are important for clays since their permeabilities are of orders of magnitude smaller than the permeability of clean sands.

There is a third surface conductance, not considered in the present theory, that adds to C_{em} and C_{os} (Pride, personal communication). This contribution is due to protons moving in the ice-like surface layers of water that are considered to be part of the solid grains and not part of the Debye layer. In soils having significant secondary clay growths (so that the grains have significant surface area), this contribution is significant at both low and high frequencies. In clean sands, this mechanism is not important.

A.2. Complex dielectric permittivity

A number of models have been proposed to determine the electromagnetic properties of composites. One such model, the complex refractive index method (CRIM) (e.g., Knight and Endres, 1990), states that

$$\epsilon(\omega) = \left(\sum_\alpha \phi_\alpha \sqrt{\epsilon_\alpha(\omega)}\right)^2, \qquad (A-11)$$

where ω is the angular frequency and ϕ_α and ϵ_α are the volume fraction and complex permittivity of the α phase, respectively. This model is very simple and of easy implementation. It uses the ray approximation in dielectrics. (The travel time in phase α is inversely proportional to the electromagnetic velocity, which in turn is inversely proportional to the square root of the dielectric constant.)

In the self-similar model (Sen et al., 1981; Feng and Sen, 1985; Carcione and Seriani, 2000), the dielectric permittivity of the composite, ϵ, satisfies

$$0 = \sum_\alpha \phi_\alpha \frac{\epsilon - \epsilon_\alpha}{2\epsilon + \epsilon_\alpha}, \qquad (A-12)$$

where ϕ_α and ϵ_α are the volume fraction and dielectric permittivity of the α phase, respectively. As Feng and Sen (1985) point out, a water-wet rock that remains percolating for small values of the porosity can be obtained from the assumption that water is the starting host material into which infinitesimal amounts of spheres of matrix and fluids are gradually included. This model is in agreement with Archie's law, i.e., it preserves the continuity of the water phase. For two constituents, the solution is given by

$$\phi_2 = f(\epsilon, \epsilon_1, \epsilon_2) = \left(\frac{\epsilon_1 - \epsilon}{\epsilon_1 - \epsilon_2}\right)\left(\frac{\epsilon_2}{\epsilon}\right)^W, \qquad (A-13)$$

where ϕ_2 is the proportion of material 2 (the host medium) and $W = 1/3$ for spherical inclusions. When $W \neq 1/3$, we have the Hanai–Bruggeman relationship (Schön, 1996, p. 473), which describes a porous medium of arbitrary grain shape.

The subsoil sediment is composed of quartz grains, clay, air, water, and contaminant. We use the Hanai–Bruggeman equation four times to obtain the complex dielectric permittivity of the sediment. The mixing order is the following: sand/clay (solid), air/contaminant (fluid 1), water/fluid 1 (fluid), and solid/fluid. If ϕ_s, ϕ_c, ϕ_w, ϕ_h, and ϕ_a denote the sand, clay, water, contaminant, and air proportions, respectively, the respective saturations are given by $S_w = \phi_w/\phi$, $S_h =$

ϕ_h/ϕ, and $S_a=\phi_a/\phi$, where $\phi=\phi_w+\phi_h+\phi_a$ is the porosity of the soil. Then, the successive application of the Hanai–Bruggeman equation implies

$$\frac{\phi_c}{\phi_c+\phi_s}=f(\epsilon_{solid},\epsilon_s,\epsilon_c),$$

$$\frac{S_a}{S_a+S_h}=f(\epsilon_{fluid\ 1},\epsilon_h,\epsilon_a),$$

$$S_w=f(\epsilon_{fluid},\epsilon_{fluid\ 1},\epsilon_w),$$

$$\phi=f(\epsilon,\epsilon_{solid},\epsilon_{fluid}), \qquad (A-14)$$

where ϵ is the complex dielectric constant of the whole soil.

For quartz and NAPL, the complex dielectric permittivity is given by

$$\epsilon=\epsilon^{\infty}+\frac{i\sigma}{\omega}, \qquad (A-15)$$

where ϵ^{∞} is the optical dielectric permittivity and σ is the dc conductivity. The complex dielectric properties of water and clay are described by the Cole–Cole model (Cole and Cole, 1941; Taherian et al., 1990):

$$\epsilon=\epsilon^{\infty}+\frac{\epsilon^{0}-\epsilon^{\infty}}{1-(i\omega\tau)^{q}}+\frac{i\sigma}{\omega}, \qquad (A-16)$$

where ϵ^0 is the static dielectric permittivity. For water (Schön, 1996, p. 398),

$$\epsilon_w^0=80.1\epsilon_0,\quad \epsilon_w^{\infty}=4.23\epsilon_0,\quad \tau_w=9.3\ \text{ps},\quad q_w=0.987;$$

and for clay,

$$\epsilon_c^0=40\epsilon_0,\quad \epsilon_c^{\infty}=30\epsilon_0,\quad \tau_c=9\ \text{ps},\quad q_c=0.9.$$

Appendix B. White's P-wave velocity for patchy saturation

White (1975) assumed spherical patches much larger than the grains but much smaller than the wavelength. He developed the theory for a gas-filled sphere of porous medium of radius a located inside a water-filled sphere of porous medium of outer radius b ($a<b$). Let us denote the saturation of gas and water by S_1 and S_2, respectively. Then

$$S_1=\frac{a^3}{b^3},\quad S_2=1-S_1. \qquad (B-1)$$

The complex velocity is given by

$$V_P=\sqrt{\frac{K+4\mu_m/3}{\rho}}, \qquad (B-2)$$

where K is the complex bulk modulus (given below), μ_m is the dry-soil shear modulus, and ρ is the composite density.

The composite density is given by

$$\rho=(1-\phi)\rho_s+\phi\rho_f, \qquad (B-3)$$

where ρ_s is the grain density, ϕ is the porosity,

$$\rho_f=S_g\rho_{f1}+(1-S_g)\rho_{f2}, \qquad (B-4)$$

and ρ_{f1} and ρ_{f2} are the densities of fluid 1 and fluid 2 (gas and water in White's theory).

Assuming that the dry-soil and grain moduli, and permeability, κ, of the different regions are the same, the complex bulk modulus as a function of frequency is given by

$$K=\frac{K_{\infty}}{1-K_{\infty}W}, \qquad (B-5)$$

where

$$W=\frac{3ia\kappa(R_1-R_2)}{b^3\omega(\eta_1Z_1-\eta_2Z_2)}\left(\frac{K_{A1}}{K_1}-\frac{K_{A2}}{K_2}\right),$$

$$R_1=\frac{(K_1-K_m)(3K_2+4\mu_m)}{K_2(3K_1+4\mu_m)+4\mu_m(K_1-K_2)S_1},$$

$$R_2=\frac{(K_2-K_m)(3K_1+4\mu_m)}{K_2(3K_1+4\mu_m)+4\mu_m(K_1-K_2)S_1},$$

$$Z_1=\frac{1-\exp(-2\gamma_1a)}{(\gamma_1a-1)+(\gamma_1a+1)\exp(-2\gamma_1a)},$$

$$Z_2=\frac{(\gamma_2b+1)+(\gamma_2b-1)\exp[2\gamma_2(b-a)]}{(\gamma_2b+1)(\gamma_2a-1)-(\gamma_2b-1)(\gamma_2a+1)\exp[2\gamma_2(b-a)]},$$

$$\gamma_j = \sqrt{i\omega\eta_j/(\kappa K_{Ej})},$$

$$K_{Ej} = \left[1 - \frac{\alpha K_{fj}(1 - K_j/K_s)}{\phi K_j(1 - K_{fj}/K_s)}\right] K_{Aj},$$

$$K_{Aj} = \left[\frac{\phi}{K_{fj}} + \frac{1}{K_s}(\alpha - \phi)\right]^{-1}, \qquad j = 1, 2,$$

$$\alpha = 1 - \frac{K_m}{K_s}, \tag{B-6}$$

K_s is the bulk modulus of the grains, K_{fj} are the bulk moduli of the fluids, η_j are the fluid viscosities, and

$$K_\infty = \frac{K_2(3K_1 + 4\mu_m) + 4\mu_m(K_1 - K_2)S_1}{(3K_1 + 4\mu_m) - 3(K_1 - K_2)S_1} \tag{B-7}$$

is the—high frequency—bulk modulus when there is no fluid flow between the patches. For a clay-free sand, K_1 and K_2 are the—low frequency—Gassmann moduli, which are given by

$$K_j = \frac{K_s - K_m + \phi K_m(K_s/K_{fj} - 1)}{1 - \phi - K_m/K_s + \phi K_s/K_{fj}}, \qquad j = 1, 2, \tag{B-8}$$

where K_m is the dry-soil bulk modulus.

We should be aware of the limitations of the theory. For simplicity in the calculations, White considers an outer sphere of radius b ($b>a$), instead of a cube. Thus, the system consists of two concentric spheres, where the volume of the outer sphere is the same as the volume of the original cube. The outer radius is $b = l/(4\pi/3)^{1/3}$, where l is the size of the cube. The distance between pockets is l. When $a = l/2$, the gas pockets touch each other. This happens when $S_1 = \pi/6 = 0.52$. Therefore, for values of the gas saturation higher than these critical values, or values of the water saturation between 0 and 0.48, the theory is not rigorously valid. Another limitation to consider is that the size of gas pockets should be much smaller than the wavelength, i.e., $a \ll c_r/f$, where c_r is a reference velocity and f is the frequency.

B.1. A simple model for clayey sands

For clayey sands, we use an effective average for the grain bulk moduli K_s and μ_s. If K_q and K_c are the sand-grain and clay-particle bulk moduli, we assume that K_s is equal to the average of the upper and lower Hashin–Shtrikman bounds. The same approach is used for the shear modulus.

Defining the porosity ϕ, the sand fraction ϕ_s, the clay fraction ϕ_c, and the clay content C, the following relations hold

$$\phi + \phi_s + \phi_c = 1 \text{ and } C = \frac{\phi_c}{\phi_c + \phi_s}. \tag{B-9}$$

The Hashin–Shtrikman upper bounds for the bulk modulus are given in Section 4.1 of Mavko et al. (1998, p. 106). According to the present notation, their symbols should be substituted as $K_1 \to K_q$, $K_2 \to K_c$, $\mu_1 \to \mu_q$, $\mu_2 \to \mu_c$, $f_1 \to 1 - C$, and $f_2 \to C$. The lower bounds are computed according to the convention indicated in the book.

The average grain density is simply $\rho_s = (1 - C)\rho_{s1} + C\rho_{s2}$, where ρ_{s1} and ρ_{s2} are the densities of quartz and clay, respectively. In this work, we assume $K_q = \mu_q = 39$ GPa, and $K_c = \mu_c = 20$ GPa.

The presence of clay also affects the dry-soil bulk and shear moduli. The porosity dependence of the dry-soil moduli is consistent with the concept of critical porosity since the moduli should vanish above a certain value of the porosity (usually from 0.4 to 0.5). This dependence is determined by the empirical coefficient A (see Eq. (B-10)). This relation was suggested by Krief et al. (1990) and applied to sand/clay mixtures by Goldberg and Gurevich (1998). Moreover, in some soils, there is an abrupt change of soil-matrix properties with the addition of a small amount of clay, attributed to softening of cements, clay swelling, and surface effects. That is, the wave velocities decrease significantly when the clay content increases from zero to a few percentages (Goldberg and Gurevich, 1998). In order to model this effect, we multiply the shear modulus of the sand matrix by a factor depending on the empirical coefficient a (see Eq. (B-11)) (this factor tends to be 1 when $a \to \infty$). Then, the bulk and shear moduli of the sand matrix is assumed to satisfy

$$K_m = K_s(1 - \phi)^{1 + A/(1-\phi)}, \tag{B-10}$$

and

$$\mu_m = \exp\{-[(1 - C)C]^a\} K_m \mu_s / K_s, \tag{B-11}$$

respectively. The values $A=2$ and $a=0.5$ are obtained by fitting the data reported by Han et al. (1986) (see Carcione et al., 2000).

Alternatively, the dry-soil moduli K_m and μ_m can be obtained, for instance, from laboratory measurements in dry samples. If c_P and c_S are the experimental dry-soil compressional and shear velocities, the moduli are given approximately by

$$K_m = (1-\phi)\rho_s\left(c_P^2 - \frac{4}{3}c_S^2\right), \quad \mu_m = (1-\phi)\rho_s c_S^2. \tag{B-12}$$

The shear modulus of the soil is not affected by the presence of fluids. The shear complex velocity is that obtained by Biot (e.g., Carcione, 2001, p. 260),

$$V_S = \sqrt{\frac{\mu_m}{\rho - \rho_f^2[m - i\eta_f/(\omega\kappa)]^{-1}}}, \tag{B-13}$$

where ρ is the composite density (see Eq. (B-3)),

$$m = \frac{\rho_f \mathcal{T}}{\phi}, \tag{B-14}$$

$\eta_f = S_g\eta_g + (1-S_g)\eta_w$, and $\mathcal{T}$ is the soil tortuosity.

B.2. Attenuation and viscodynamic effects

Additional attenuation is described with the constant Q model and viscodynamic functions to model the high-frequency behavior. Constant Q models provide a simple parameterization of seismic attenuation in rocks in oil exploration and in seismology. By reducing the number of parameters, they allow an improvement of seismic inversion. Moreover, there is physical evidence that attenuation is almost linear with frequency (therefore Q is constant) in many frequency bands. The attenuation kernel corresponding to a constant Q over all frequencies is (e.g., Carcione, 2001, p. 73)

$$M(\omega, Q) = \left(\frac{i\omega}{\omega_0}\right)^{2\gamma}, \quad \gamma = \frac{1}{\pi}\tan^{-1}\left(\frac{1}{Q}\right) \tag{B-15}$$

where ω is the angular frequency and ω_0 is a reference frequency. Attenuation is modeled by making viscoelastic the White bulk and shear moduli. We set

$$K \to KM(\omega, Q_\kappa),$$

$$\mu_m \to \mu_m M(\omega, Q_\mu), \quad Q_\mu = \left(\frac{\mu_m}{\mathrm{Re}(K)}\right)Q_\kappa, \tag{B-16}$$

where Q_κ is a free parameter. Eq. (B-16) implies that the lower the modulus, the higher the attenuation. Choosing the reference frequency at high frequencies implies that the velocity for lower frequencies is lower than the velocity given by White's model in the absence of viscoelastic attenuation.

High-frequency viscodynamic effects imply the substitution

$$\eta_j \to \eta_j F_j(\omega), \qquad j = 1, 2. \tag{B-17}$$

Johnson et al. (1987) obtained an expression for the viscodynamic function, which provides a good description of both the magnitude and phase of the exact dynamic tortuosity of large networks formed from a distribution of random radii.

The viscodynamic functions are

$$F_j(\omega) = \sqrt{1 + \frac{4i\mathcal{T}^2\kappa}{x_j\Lambda^2\phi}}, \qquad x_j = \frac{\eta_j\phi}{\omega\kappa\rho_{fj}}, \; j = 1, 2 \tag{B-18}$$

(Johnson et al., 1987; Carcione, 2001, p. 252), where Λ is a geometrical parameter, with $2/\Lambda$ being the surface-to-pore volume ratio of the pore–solid interface. The following relation between $\mathcal{T}$, κ, and Λ can be used:

$$\frac{\xi\mathcal{T}\kappa}{\phi\Lambda^2} = 1, \tag{B-19}$$

where $\xi = 12$ for a set of canted slabs of fluid and $\xi = 8$ for a set of nonintersecting canted tubes.

References

Akbar, N., Mavko, G., Nur, A., Dvorkin, J., 1994. Seismic signatures of reservoir transport properties and pore fluid distribution. Geophysics 59, 1222–1236.

Angenheister, G. (Ed.), 1982. In: Landolt-Börnstein, Hellwege,

K.H. (Eds.), Physical Properties of Rocks, vol. 1b. Springer-Verlag, Berlin.

Archie, G.E., 1942. The electrical resistivity log as an aid in determining some reservoir characteristics. Trans. AIME 146, 54–62.

Cadoret, T., Marion, D., Zinszner, B., 1995. Influence of frequency and fluid distribution on elastic wave velocities in partially saturated limestones. J. Geophys. Res. 100, 9789–9803.

Carcione, J.M., 1996a. Ground-penetrating radar: wave theory and numerical simulation in lossy anisotropic media. Geophysics 61, 1664–1677.

Carcione, J.M., 1996b. Ground radar simulation for archaeological applications. Geophys. Prospect. 44, 871–888.

Carcione, J.M., 2001. Wave Fields in Real Media: Handbook of Geophysical Exploration, vol. 31. Pergamon, Amsterdam.

Carcione, J.M., Seriani, G., 2000. An electromagnetic modelling tool for the detection of hydrocarbons in the subsoil. Geophys. Prospect. 48, 231–256.

Carcione, J.M., Gurevich, B., Cavallini, F., 2000. A generalized Biot–Gassmann model for the acoustic properties of shaley sandstones. Geophys. Prospect. 48, 539–557.

Carmichael, R.S., 1989. Physical Properties of Rocks and Minerals. CRC Press, Florida.

Clark Jr., S.P., 1966. Handbook of Physical Constants. Yale Univ. Press, New York.

Clement, W.P., Cardimona, S., Endres, A.L., Kadinsky-Cade, K., 1997. Site characterization at the groundwater remediation field laboratory. Lead. Edge 16, 1617–1621 (November).

Cole, K.S., Cole, R.H., 1941. Dispersion and absorption in dielectrics. J. Chem. Phys. 9, 341–351.

Daniels, J.J., Roberts, R., Vendl, M., 1995. Ground penetrating radar for the detection of liquid contaminants. J. Appl. Geophys. 33, 195–207.

Dvorkin, J., Mavko, G., Nur, A., 1995. Squirt flow in fully saturated rocks. Geophysics 60, 97–107.

Endres, A.L., Redman, D.J., 1993. Modeling the electrical properties of porous rocks and soils containing immiscible contaminants. In: Bell, R.S., Lepper, C.M. (Eds.), Proceedings of the Symposium on the Application of Geophysics to Engineering and Environmental Problems, San Diego, pp. 21–38.

Feng, S., Sen, P.N., 1985. Geometrical model of conductive and dielectric properties of partially saturated rocks. J. Appl. Phys. 58, 3236–3243.

Goldberg, I., Gurevich, B., 1998. A semi-empirical velocity–porosity–clay model for petrophysical interpretation of P- and S-velocities. Geophys. Prospect. 46, 271–285.

Greenhouse, J., Brewster, M., Schneider, G., Redman, D., Annan, P., Olhoeft, G., Lucius, J., Sander, K., Mazzella, A., 1993. Geophysics and solvents: the Borden experiment. Lead. Edge, 261–267 (April issue).

Hagrey, S.A., Müller, C., 2000. GPR study of pore water content and salinity in sand. Geophys. Prospect. 48, 63–85.

Han, D.H., Nur, A., Morgan, D., 1986. Effects of porosity and clay content on wave velocities in sandstones. Geophysics 51, 2093–2107.

Hubbard, S.S., Peterson Jr., J.E., Majer, E.L., Zawislanski, P.T., Williams, K.H., 1997. Estimation of permeable pathways and water content using tomographic radar data. Lead. Edge 16, 1623–1628 (November).

Johnson, D.L., Koplik, J., Dashen, R., 1987. Theory of dynamic permeability and tortuosity in fluid-saturated porous media. J. Fluid Mech. 176, 379–402.

King, M.S., Marsden, J.R., Dennis, J.W., 2000. Biot dispersion for P- and S-waves velocities in partially and fully saturated sandstones. Geophys. Prospect. 48, 1075–1089.

Knight, R., Endres, A., 1990. A new concept in modeling the dielectric response of sandstones: defining a wetted rock and bulk water system. Geophysics 55, 586–594.

Krief, M., Garat, J., Stellingwerff, J., Ventre, J., 1990. A petrophysical interpretation using the velocities of P and S waves (full waveform sonic). Log Anal. 31, 355–369.

Mavko, G., Mukerji, T., Dvorkin, J., 1998. The Rock Physics Handbook: Tools for Seismic Analysis in Porous Media. Cambridge Univ. Press, Cambridge.

Pride, S., 1994. Governing equations for the coupled electromagnetics and acoustic of porous media. Phys. Rev., B 50 (21), 15678–15696.

Pride, S., Morgan, F.D., 1991. Electrokinetic dissipation induced by seismic waves. Geophysics 56, 914–925.

Rhoades, J.D., 1980. Determining leaching fraction from field measurements of soil electrical conductivity. Agric. Water Manag. 3, 205–215.

Rhoades, J.D., Chanduvi, F., Lesch, S., 1999. Soil salinity assessment: methods and interpretation of electrical conductivity measurements. FAO Irrig. Drain. Pap. 57, 1–149.

Schön, J.H., 1996. Physical Properties of Rocks, Handbook of Geophysical Exploration. Pergamon, Oxford.

Sen, P.N., Scala, C., Cohen, M.H., 1981. A self-similar model for sedimentary rocks with applications to the dielectric constant of fused glass beads. Geophysics 46, 781–795.

Senechal, P., Perroud, H., Garambois, S., 2000. Geometrical and physical parameters comparison between GPR data and other geophysical data. In: Noon, D., Nobes, D. (Eds.), Proceedings of the Eighth International Conference on Ground Penetrating Radar, GPR 2000, Gold Coast, Australia, pp. 618–623.

Taherian, M.R., Kenyon, W.E., Safinya, K.A., 1990. Measurement of dielectric response of water-saturated rocks. Geophysics 55, 1530–1541.

Valle, S., Carcione, J.M., 2003. Detection of liquid contaminants in the subsoil using the GPR technique. J. Appl. Geophys. (in press).

Wensink, W.A., 1993. Dielectric properties of wet soils in the frequency range 1–3000 MHz. Geophys. Prospect. 41, 671–696.

White, J.E., 1975. Computed seismic speeds and attenuation in rocks with partial gas saturation. Geophysics 40, 224–232.